INSTITUTE OF PHYSICS PUBLISHING SMART MATERIALS AND STRUCTURES
Smart Mater. Struct. **16** (2007) S108–S114 doi:10.1088/0964-1726/16/1/S11

# Shape memory and martensite deformation response of $Ni_2MnGa$

**J D Callaway[1], R F Hamilton[1], H Sehitoglu[1,4], N Miller[1], H J Maier[2] and Y Chumlyakov[3]**

[1] Department of Mechanical Science and Engineering, University of Illinois at Urbana-Champaign, Urbana, IL 61801, USA
[2] University of Paderborn, Lehrstuhl für Werkstoffkunde, D-33098 Paderborn, Germany
[3] Siberian Physical Technical Institute, Novosoborny Square 1, Tomsk, 634050, Russia

E-mail: huseyin@uiuc.edu

Received 10 August 2005, in final form 17 February 2006
Published 15 January 2007
Online at stacks.iop.org/SMS/16/S108

**Abstract**
The purpose of this paper is twofold: to establish the magnitude of detwinning stress levels of non-modulated martensite in $Ni_{53}Mn_{25}Ga_{22}$ as a function of heat treatments utilizing single crystals, and to study the shape memory strains from constant-load temperature cycling experiments for aged and unaged conditions. The maximum transformation strains of 5.2% are consistent with the theoretical predictions based on energy minimization theory. The results exhibit a remarkable narrowing of the thermal hysteresis (as low as 2 °C) with increasing applied stress and a considerable two-way shape memory effect. Using microscopy, it is shown that aging produces a finer martensitic plate structure with an accompanying increase in detwinning stress compared to the unaged case.

## 1. Introduction

Ferromagnetic shape memory alloys possess the unique ability to achieve large, reversible strains due to variant reorientation caused by the application of a magnetic field, and can also be utilized as shape memory alloys undergoing reversible phase transformations. Despite the recent surge of interest in the magnetic shape memory (MSM) properties of $Ni_2MnGa$ [1–3], only limited information [4–7] pertinent to the use of the alloy as a conventional shape memory metal has been presented. However, these publications were not written for the purpose of characterizing the conventional shape memory behavior exclusively. Consequently, they do not provided a complete analysis evaluating and interpreting stress–strain results, differential scanning calorimetry (DSC), two-way shape memory effect (TWSME) and microscopy results in one comprehensive study. In this paper, we focus on (i) the effects of heat treatment on the detwinning stress as a function of temperature, and (ii) the strain–temperature behavior resulting from the thermally induced austenite to martensite transformation under constant stress. Additionally, a discussion of the material's two-way shape memory behavior with different thermal treatment history is presented and discussed.

For the chemical composition chosen in this work, a non-modulated (NM) structure exists, which has the potential of producing the largest detwinning strains. It has been reported that the twinning stress for $Ni_2MnGa$ martensite is higher than 10 MPa for NM martensite [3]. We explore the stress at the onset of detwinning and demonstrate that the stress level does not exhibit a plateau but a considerable increase with increasing deformation. The martensite plate width and twin lamellae size is found to change with aging in this class of alloys. This work discusses the effect of this microstructural change on the mechanical response.

For notable recoverable deformation to occur due to either applied magnetic fields or applied stresses [2], significant variant reorientation and detwinning, i.e. the growth of one group of twins at the expense of others, must occur. A fundamental and critical property in shape memory alloys is the recoverability of transformation strain, albeit with transformation hysteresis [8]. The hysteresis observed in martensitic transformations results from energy dissipative (irreversible) processes. In order to understand the magnitude of the stress levels to induce recoverable martensitic transformation (MT) a series of experiments under

[4] Author to whom any correspondence should be addressed.

constant stress while thermal cycling were undertaken. Such information has been missing in the literature and explores the potential use of these materials for shape memory applications requiring low thermal hysteresis. The results show that the transformation is reversible with a small hysteresis (as low as 2 °C) and the magnitude of stresses to induce saturation transformation strains due to the MT are as low as 25 MPa for the unaged case. The DSC results confirm the narrowing of the thermal hysteresis associated with the aging. In addition, we demonstrate a two-way shape memory effect for a heat treated and an unaged sample. While MSM applications require very low detwinning stresses, other shape memory alloy applications such as those currently utilizing NiTi may desire a strong material with a narrow thermal hysteresis. NiTi alloys exhibit a thermal hysteresis of approximately 30 °C [9], compared to less than 2 °C in these $Ni_2MnGa$ alloys. Therefore, a study of the stress levels in the martensitic domain along with the thermal hysteresis behavior of higher strength $Ni_2MnGa$ alloys warrants further consideration.

In summary, we classify the mechanical response below the austenite to martensite transition temperature through the use of stress–strain experiments and thermal cycling experiments under stress. We study the thermally induced MT in the absence of an external load with DSC results.

The results shown in this work illustrate the potential utility of these materials for a broader range of applications. The narrow thermal hysteresis indicates that this material could be used for a quick-response thermal driven actuator. We show that the aged and unaged material achieve similar maximum transformation strains; however, the unaged material reaches the strain at a higher stress and thus allows for application optimization. Aging drives an increase in the detwinning stress, indicating that thermal treatments can be used to tailor the martensitic mechanical response to meet the needs of high strain shape recovery applications (up to 18% strain [3]).

## 2. Material and experimental techniques

Single-crystal $Ni_{53}Mn_{25}Ga_{22}$ at.% ingots were grown using the Bridgman technique in an inert environment. Rectangular specimens were then cut from the ingot into 4 mm × 4 mm × 10 mm samples with the [001] direction longitudinally oriented and the (100) plane oriented parallel to a side face. Chemical analysis was performed on the material before and after crystal growth due to a concern for the loss of Mn content during the crystal growth process. The chemistry measured after crystal growth indicated a 0.5% loss of Mn, which did not alter the modulation of the martensite. The loss of Mn slightly altered the free electron to atom ($e/a$) ratio, resulting in a small shift of the transformation temperatures (approximately 10 K) [10]. Chemistry reported in this work represents results from the post-growth analysis after the specimens were oriented and cut. Using a low speed saw, single-crystal DSC samples, each with a mass of approximately 80 mg, were sectioned from the bulk rectangular specimens.

Stress–strain behavior was measured in compression along the [001] direction. Mechanical testing was performed on an Instron 8802 servohydraulic load frame. Load and strain measurements were transduced from an Instron Dynacell load cell and an MTS miniature extensiometer with 3 mm gauge length, respectively. Temperature was manually controlled using a liquid nitrogen heat exchanger and an induction heater. Prior to the constant load temperature cycling, the specimens were heated well above $A_f$ to ensure that the load was applied in a fully austenitic condition. Data were then recorded during cooling to the lowest temperature and subsequent heating back to the test start temperature.

DSC experiments were performed using a Perkin Elmer Instruments Pyris 1 DSC. Heating and cooling rates for the DSC testing were maintained at 40 °C min$^{-1}$. A heating and cooling rate of approximately 40 °C min$^{-1}$ was also used for the constant stress–temperature cycling tests. The high DSC temperature ramp rate has the effect of increasing the measured enthalpy of transformation [11]. Higher measured transformation enthalpy leads to enhancement of peaks and therefore to results with more distinguished features useful for comparing the results of similar materials (or heat treatments).

Heat treatment of the material was conducted in a Lindberg/Blue air furnace and the resulting oxide layer was removed. Electropolishing required for microscopy was conducted using a solution of 33% nitric acid and methanol. Optical microscopy was performed on several specimens using an Olympus BX51M microscope.

## 3. Experimental results

Heat treatments were conducted on DSC specimens at several temperatures including 980, 950, 900, 850 and 800 °C. Annealing times were each selected to be 24 h, except for the 980 °C case, which was for 30 h and was followed by an 800 °C, 20 h treatment. Heat treatment temperatures were selected to be near the ordering temperature (approximately 800 °C) suggested by Overholser [12]. Heat treatment durations were selected to supply ample time for long range ordering to occur. The heat treatments selected are among some of the common thermal treatment procedures used in the study of $Ni_2MnGa$ alloys [3, 13–19]. The selection of the heat treatments allowed for a systematic evaluation of the transformation temperatures and detwinning stress levels. The role of different cooling rates was examined by comparing the DSC results for a water quench and a slow furnace cool.

The DSC results show that heat treatments over 900 °C reduced the magnitude of the transformation peaks to the point where no detectable peaks were identified for the 980 °C heat treatment. A summary of the results is displayed in table 1. The magnitude of the area under the peak reflects the enthalpy of transformation. The enthalpy of transformation decreased significantly for all the heat treatments compared with that of the unaged sample. The 900 °C heat treatments showed approximately 50% less transformation enthalpy than the 800 °C heat treatment and 66% less than the unaged case. The quenching method also affects the transformation enthalpy, but to a lesser degree. The furnace cooled specimens exhibited 21% more transformation enthalpy than the water quenched samples with the largest effect seen for the 850 °C case.

The thermal hysteresis was measured from peak to peak on the DSC curves in order to avoid ambiguity in the value selection. All heat treatments lowered the thermal hysteresis relative to the unaged condition. The reduction in thermal

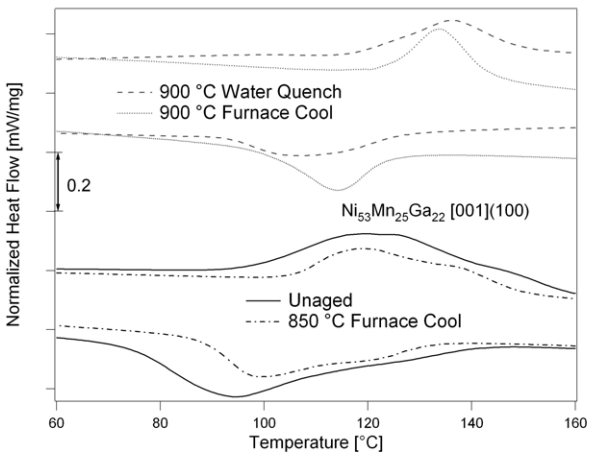


**Figure 1.** DSC results for $Ni_{53}Mn_{25}Ga_{22}$ at.% for several heat treatments, including unaged. All heat treatments plotted are for 24 h.

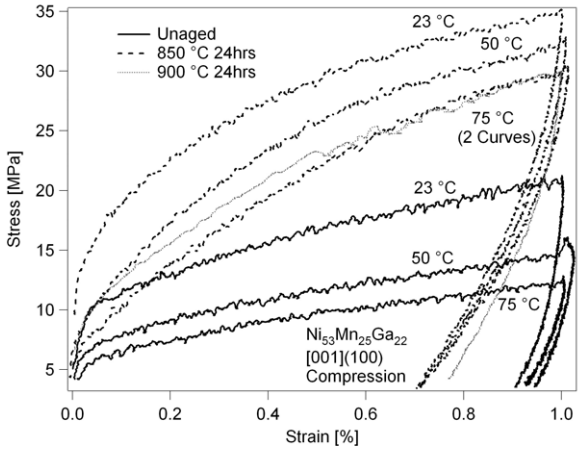


**Figure 2.** Compressive stress versus strain results for $Ni_{53}Mn_{25}Ga_{22}$ at.% displaying curves for 850 and 900 °C furnace cooled samples and an unaged sample. Note that only the data for the 75 °C test on the 900 °C heat treatment are shown to reduce overlap.

**Table 1.** Summary of DSC results for several heat treatments. All heat treatments are for 24 h with the exception of the 980 °C, 30 h followed by 800 °C, 20 h treatment.

| Heat treatment (°C) | Quenching method | Temperature hysteresis (°C) | Enthalpy of transformation (J $g^{-1}$) |
|---|---|---|---|
| None | N/A | 31 | 9.65 |
| 800 | Water quench | 16 | 5.84 |
| 800 | Furnace cool | 19 | 7.75 |
| 850 | Water quench | 19 | 3.91 |
| 850 | Furnace cool | 21 | 6.16 |
| 900 | Water quench | 29 | 3.17 |
| 900 | Furnace cool | 20 | 3.46 |
| 950 | Water quench | 18 | 0.51 |
| 950 | Furnace cool | 17 | 0.60 |
| 980, 800 | Water quench | N/A | N/A |

hysteresis observed with DSC is also apparent in the strain–temperature results as discussed later. The DSC results for four selected thermal treatments are shown in figure 1. The heat treatments selected for stress–strain experiments demonstrate relatively low thermal hysteresis and different DSC peak contours, while still exhibiting a high enthalpy of transformation per unit volume.

To study the stress–strain response three conditions were examined: a specimen with no heat treatment after single-crystal growth and specimens aged at 850 and 900 °C, both followed by a furnace cool. The specimen with no post-crystal growth heat treatment is referred to as unaged.

The 850 °C heat treatment showed very similar martensitic stress–strain curves (figure 2) compared to 900 °C; consequently no lower temperature treatments were examined. Only one 900 °C stress–strain curve is presented for reference. At some lower temperature range a transition would be expected for the aged response to approach that of the unaged case. No additional tests were conducted on samples aged at temperatures above 900 °C because the DSC results indicated a substantial reduction in the enthalpy of transformation per unit volume.

The stress–strain response was established at temperatures of 23, 50 and 75 °C, each below the martensite finish temperature, $M_f$. Residual martensitic strain recovery was performed for each case by heating the specimen over 130 °C, beyond $A_f$, at zero load with full recovery. The martensitic detwinning stress is a strong function of the testing temperature, reaching a minimum at approximately 75 °C for all the tested samples. The aged specimens show a higher degree of hardening than the unaged specimen, especially near the $M_s$ temperature. The detwinning stress, measured using an intersecting slopes method, increased due to the heat treatment of the material. The detwinning stress for 75 °C is 7 MPa for the unaged specimen, 11 MPa for the 850 °C and 12 MPa for the 900 °C aged case. The detwinning stresses at 23 °C for unaged and 850 °C aged were 13 and 24 MPa, respectively. We note the high sensitivity of the martensitic twinning on the testing temperature.

Figure 3 depicts strain–temperature curves for the unaged and aged conditions. In this set of experiments the applied stress is maintained constant and the temperature is cycled. The material transforms from an austenitic to martensitic structure in a reversible fashion. The thermal hysteresis at small loads is lower for the aged sample. The transformation strains at 3 MPa are similar for both virgin specimens. The unaged sample showed progressively lower thermal hysteresis as the load was increased, showing only 4 °C at 25 MPa. Further loading of this sample brought an even lower thermal hysteresis, less than 2 °C with a 35 MPa applied compression stress, while still achieving 5% transformation strain. This is among the lowest values of temperature hysteresis reported [8, 9] for any shape memory metal. The aged sample shows relatively small amounts of thermal hysteresis at low stress, but the hysteresis increases as the stress increases. At 25 MPa the hysteresis reaches 12.5 °C, and then begins to decrease down to 7.5 °C at 60 MPa. Both materials saturated at the same strain of approximately 5.2%, but the aged specimen required more than double the stress of the unaged to reach this peak transformation strain. The two-way shape memory response of the samples after the thermal cycling at high stress is presented as dashed lines in figure 3. It is important to note that a 3 MPa compressive stress was

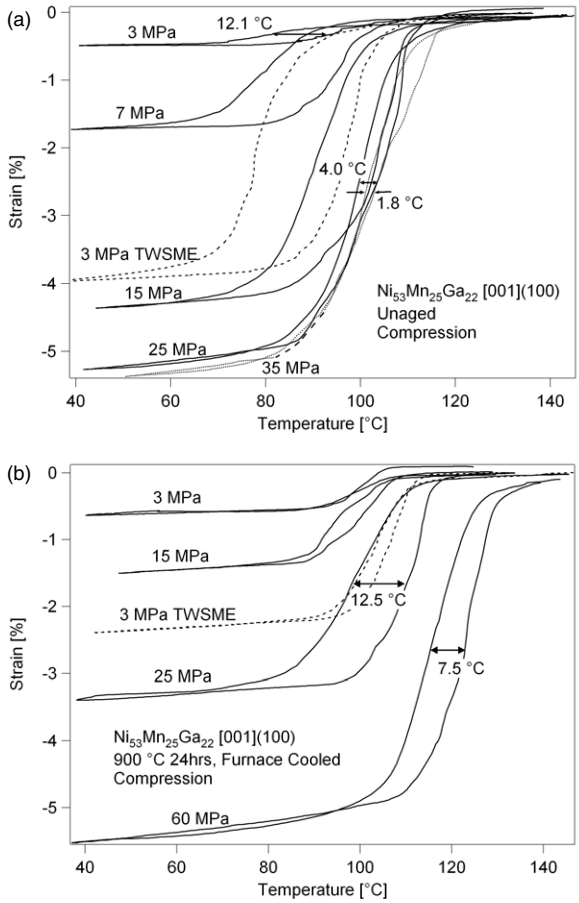


**Figure 3.** (a) Strain–temperature results for unaged $Ni_{53}Mn_{25}Ga_{22}$ at.%. The dashed curve depicts the TWSME after thermal cycling. (b) Strain–temperature results for $Ni_{53}Mn_{25}Ga_{22}$ at.% aged at 900 °C for 24 h followed by a furnace cool. Compare the thermal hysteresis for the two samples.

applied during this testing to hold the sample in place in the load frame. Since this relatively small compressive stress was applied consistently to each specimen, it does not alter the comparisons made from the results. The TWSME strain was 2.2% for the 900 °C treated sample and 3.8% for the unaged specimen as reported in table 2. The TWSME thermal hysteresis is 18.9 °C for the unaged sample and 2.9 °C for the aged specimen. The saturation transformation strain measured in this alloy was also compared to theoretical results calculated using lattice parameters, as discussed in the following.

The $Ni_2MnGa$ alloy considered in this work undergoes a MT from a face-centered cubic (fcc) $L2_1$ austenite phase to a face-centered tetragonal (fct) $L1_0$ martensitic phase that is non-modulated. For the fcc to fct MT there are three independent lattice correspondences [20, 21] yielding three martensite variants. The deformation matrices to obtain these variants, defined in the austenite coordinate system, are designated $\boldsymbol{U}_1$, $\boldsymbol{U}_2$ and $\boldsymbol{U}_3$ and the components are functions of the $L2_1$ and $L10$ lattice parameters as defined in [20]. Two martensite variants in twin relation to one another constitute a correspondence variant pair (CVP). We calculate the theoretical transformation strain for a CVP using a framework based on the energy minimization theory

**Table 2.** Summary of martensite to austenite transformation strains showing theoretical maximum strain and experimental results.

| Theoretical trans. strain | Exp. trans. strain under stress | TWSME strain |
|---|---|---|
| 6.6% | 5.2% unaged | 3.8% unaged |
| | 5.1% aged 900 °C | 2.2% aged 900 °C |

(EMT) [22]. The EMT has been utilized in previous studies to predict the orientation dependence of CVP strains for Fe–Ni–Co–Ti [21, 23] and Co–Ni–Al [24, 25], which undergo cubic to tetragonal MTs. Sehitoglu *et al* [23, 25] provide a review of the EMT, and the results from the current analysis are summarized next.

In the present work, the CVP habit (invariant) plane orientations and transformation directions, and the twin parameters within the CVP are established for $Ni_2MnGa$ with the lattice parameters $a_0 = 5.82$ Å [4], $c = 6.58$ Å and $a = 5.46$ Å [3]. The twin plane and twin shear vectors are $\boldsymbol{n} = (0, 0.7071, -0.7071)$, and $\boldsymbol{a} = (0, 0.2447, 0.2949)$. The volume fraction of variants within a martensite CVP is $f = 0.3487$ and $1 - f = 0.6513$. Finally, the habit plane normal and transformation directions are established as $\boldsymbol{m} = (-0.6997, 0.0962, 0.7079)$ and $\boldsymbol{b} = (0.0909, 0.0111, 0.0814)$, respectively. The transformation strain is then calculated using the large (Green) strain theory

$$\boldsymbol{\varepsilon} = \tfrac{1}{2}[\boldsymbol{b} \otimes \boldsymbol{m} + \boldsymbol{m} \otimes \boldsymbol{b} + (\boldsymbol{b} \cdot \boldsymbol{b})\boldsymbol{m} \otimes \boldsymbol{m}]. \qquad (1)$$

We present the theoretical strain calculated using equation (1) for the [001] orientation in compression obtained using EMT for NM martensite in table 2.

Subsequent to the thermal cycling, stress–strain tests were again performed on the samples. Both the aged and unaged samples displayed a slightly lower detwinning stress. However, both specimens also displayed a significantly higher hardening rate after high stress thermal cycling. These results are not included for the sake of brevity.

Figure 4 shows optical microscopy pictures taken from the 900 °C aged and the unaged specimens. Both figures correspond to the same magnification, as noted by the micron bar, detailing the differences in martensite morphology. The constant stress load cycling testing was performed on the depicted specimens prior to obtaining the images. The martensite images are indicative of the typical microstructure found on the specimens. Note that the martensite for the 900 °C heat treatment is finer, showing interacting variants. The average martensite plate thickness, labeled as $d_m$, is 4.3 $\mu$m for the unaged and 2.3 $\mu$m for the 900 °C aged samples. These values were an average of the measurement of several twin plates.

In addition to the conventional optical microscopy, we have also studied transmission electron microscopy (TEM) results for an unaged (figure 5(a)) and for an aged (figure 5(b)) sample. The NM martensite structure was verified for both the unaged and aged crystals by examining the selected area diffraction (SAD) pattern presented in the upper right corners of the images. The TEM pictures look closely at the microstructural twinning that occurs with the plates observed in figures 4(a) and (b). In contrast to that of the aged sample,

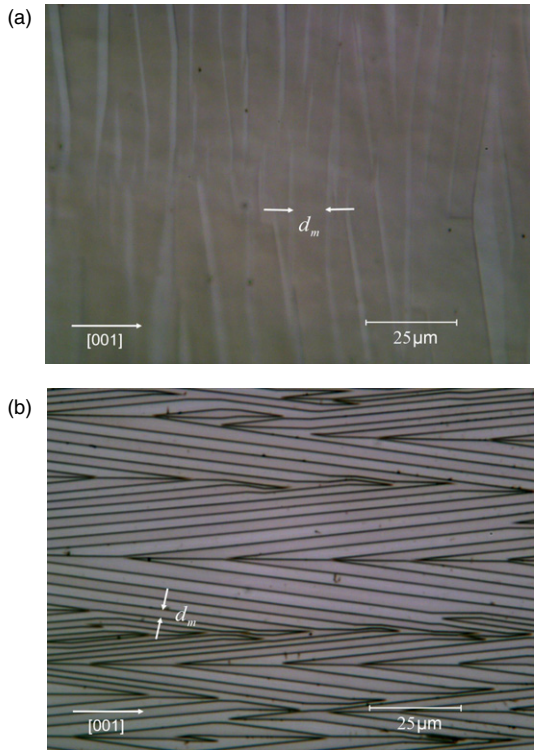


**Figure 4.** (a) Optical microscopy of an unaged $Ni_{53}Mn_{25}Ga_{22}$ at.% sample. (b) Optical microscopy of a $Ni_{53}Mn_{25}Ga_{22}$ at.% 900 °C aged sample. Note that the plate thickness is smaller in this case.

the unaged sample shows a coarser twin lamellae structure throughout. We have noted the twin lamellae thickness in each image by $d_{\text{lam}}$. In addition, the unaged sample shows an increased density of defects, the details of which are difficult to resolve. The area encapsulated by region A depicts a rather large defect detected by the TEM. The TEM image of the aged sample details extremely fine lamellae, highlighted in area B, that form near a CVP boundary.

## 4. Discussion of results

DSC results provide a quantitative comparison between the unaged and aged transformation behavior and reveal the effect of cooling rates following heat treatment. In contrast to the definitive transformation peaks resulting from the 900 °C heat treatment, the peaks for the unaged alloy are markedly more diffuse. Previous studies that consider the effects of aging for non-stoichiometric $Ni_2MnGa$ alloys report similar trends [13–15]. In the unaged condition, for this class of alloys, compositional gradients associated with macro- and microsegregation result from single-crystal growth [15, 26]. As a result, local atomic order is disrupted yielding local changes in the $e/a$ ratio for the unaged alloy. Jin *et al* [10] and Wu and Yang [16] show that $M_s$ decreases with decreasing $e/a$ ratio. Bennett *et al* [26] note that small compositional variations of the order of 1–2% can alter the $e/a$ ratio enough to produce drastic variations in $M_s$ of 100–200 K. The broad diffuse peaks for the unaged case result from spatially heterogeneous transformations that occur at different $M_s$ temperatures that span large intervals ($M_s - M_f \approx 60$ °C).

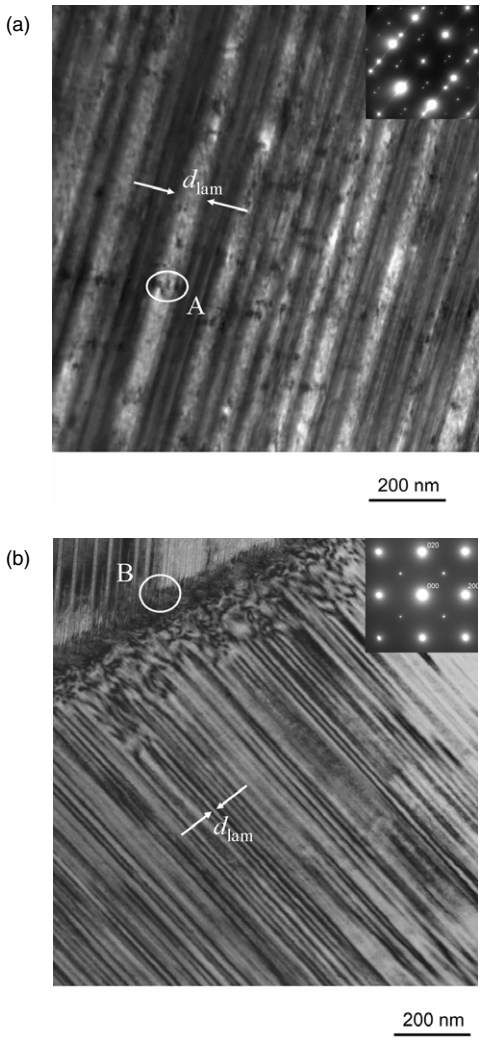


**Figure 5.** (a) TEM image of an unaged $Ni_{53}Mn_{25}Ga_{22}$ at.% sample with the SAD pattern shown in the upper right. The bright-field image was recorded under the two-beam condition, whereas the diffraction pattern was obtained from the lower part of the image after tilting to a low-index zone axis. (b) TEM image of a $Ni_{53}Mn_{25}Ga_{22}$ at.% 850 °C aged sample with SAD pattern shown in the upper right. Note the finer lamellae and the reduced number of defects.

It follows that during the reverse transformation, the peaks are diffuse and the transformation intervals are large due to the inhomogeneous elastic energy storage during the forward transformation [17].

The peaks for the 900 °C, 24 h heat treatments are markedly more distinct and occur over a considerably smaller temperature interval ($M_s - M_f \approx 25$ °C) than the unaged case indicating that the aging treatment yields a homogenized composition and leads to a higher degree of atomic order. The smaller hysteresis and lower $M_s$ temperatures for the aged cases support our assertion that aging increased the atomic order of the $Ni_{53}Mn_{25}Ga_{22}$ alloy. Ling and Owen [27] and Gao *et al* [13] assert that increased atomic ordering reduces the chemical driving force available at $M_s$, thus lowering $M_s$. More ordered alloys exhibit a higher flow stress and generation of dislocations is suppressed, which

decreases the hysteresis [13, 27]. This is substantiated by the stress versus strain results for the aged alloys (figure 2), which exhibit a higher reorientation stress than the unaged alloys. Note that the peaks corresponding to the 850 °C heat treatment are diffuse as well, revealing that the temperature is not sufficient to homogenize the composition or induce significant atomic rearrangement. However, comparing the transformation temperature interval and peak heights, the unaged transformation remains significantly more diffuse than for the 850 °C heat treatment. The presence of intermediate martensitic transformations can also cause the double peaks as seen in the 850 °C case and to a lesser degree in the unaged case, although this was not studied in this work.

We now consider the effect of cooling rate. The 900 °C heat treatment displays a much more distinct peak for furnace cooling compared with water quenching. A high concentration of vacancies resulting from rapid quenching and enhanced by the stoichiometric chemistry deviation yields high residual stresses. As a result of irreversibilities attributed to the quenched in defects, a larger hysteresis results for the water quenched specimens. The water quenched samples likely show a broader peak because of concomitant heterogeneity of the microstructure ordering and local composition as previously explained. The furnace cooled samples show a more definitive DSC peak because slower cooling drastically decreases the dislocation density, which increases the homogeneity of the microstructure [13, 18]. Note that the transformation temperatures are similar for both cooling rates. It is expected that quenched-in defects would serve as nucleation sites for martensite, thus increasing the transformation temperatures compared to the furnace cooled samples [13]. Since this is not the case, it appears that the 900 °C heat treatment temperature stabilizes the austenite, which minimizes the influence of the quenched in defects on the transformation temperatures. Indeed, Hosoda *et al* [19] report that hardness increases with increasing heat treatment temperature for near-stoichiometric $Ni_2MnGa$. For the higher temperature heat treatments (950 and 980 °C), DSC peaks were very small and diffuse, substantiating stabilization of the austenitic phase in the testing temperature regime.

Isothermal uniaxial compression stress–strain curves illustrate the influence of the different martensite plate dimensions that form for the unaged versus aged cases. A fine twinned microstructure developed with a greatly reduced martensite plate thickness as a result of heat treatments. The increased twin density in the 900 °C aged case (figure 4(b)) gives rise to a higher degree of twin interaction. The 850 °C treatment showed a microstructure very similar to the 900 °C case. A finer martensite twin plate thickness implies a strengthening in the martensite phase which is consistent with the increase in detwinning stress for the aged versus unaged results, at the same temperatures, in figure 2. Using copper-based alloys, Khan *et al* [28] suggested that a Hall–Petch type of relationship exists for martensite plate thickness with inverse square root dependence. The finer martensite microstructure formed during heat treatment resists reorientation during deformation, as suggested by the increased hardening rate in the stress–strain response.

Figures 5(a) and (b) show obvious differences between the aged and unaged microstructure within a twin variant which indicate that the observations in figure 4 exist at a much finer scale. Similar to the refinement of the martensite plate size, there is a substantial reduction in the size of twin lamellae due to aging. The high number of defects present in the TEM image of the unaged sample may alter the chemical energy significantly enough to alter the stacking of the martensite planes, thus altering the thickness of the twin lamellae. The refinement of the microstructure substantiates previous claims made regarding the effects of heat treatment on ordering and internal stress relief. The decreased number of defects and the corresponding narrowing of twin lamellae in the aged case provide additional rationale for the strengthening of the material after aging. The extremely fine lamellae seen near the CVP boundary of the aged specimen is similar to that seen in [29]. The diffraction pattern in figure 5(a) is typical for two twin related variants of NM martensite as discussed in [30]. Comparatively, the pattern in figure 5(b) is typical for an observation of a single variant of NM martensite.

To further establish the mechanical response as a function of aging for the $Ni_{53}Mn_{25}Ga_{22}$ alloy, we consider the strain–temperature results (figure 3). In the case of very low external stress such as under 3 MPa, the internal stress fields are expected to dominate and influence the transformation strains and the thermal hysteresis. It is likely that single-crystal growth induces residual internal stress fields, which alter martensite variant morphology, that are relieved by the aging treatment. This claim is substantiated by TEM imaging that indicates wider twins and more defects in the unaged material, both of which are often associated with higher internal stress fields. Therefore, the unaged sample shows significantly larger thermal hysteresis (near 12 °C) at 3 MPa compared to the aged sample (<2 °C). Larger thermal hysteresis is often associated with increased interaction of internal stress and external stress induced martensite and dissipation at the austenite–martensite interfaces. The result raises the possibility that the dislocations inherent to the transformation are considerably less influential for the aged case and, in light of the strengthening of the matrix, due to the twin size refinement after aging elastic accommodation is enhanced. When the applied stress on the unaged sample is increased during temperature cycling, the hysteresis increases under the 7 MPa stress and thereafter experiences a significant reduction. The aged samples display a gradual increase up to 25 MPa that is also followed by a decrease in hysteresis. We consider the stress at which the hysteresis obtains a maximum value as the external stress required to overcome internal stresses and create a stable dislocation arrangement. After this stress is reached, residual stress fields due to residual martensite and/or transformation dislocations could become more biased toward the external stress and assist the transformation for subsequent cycles. Consequently, the hysteresis decreases and transformation temperatures increase.

The resultant transformation strains in both cases are similar (less than 6%) and very close in magnitude. For each stress level up to saturation the unaged specimen shows a higher transformation strain. We note that the aged sample required a higher external stress to reach the saturation transformation strain of 5%. This can be attributed to the previously discussed strengthening mechanisms for the aged case. The discrepancy between the theoretical transformation strains and the experimental strains listed in

table 2 arise because the EMT considers interfaces that are coherent with the matrix. When transformation strains are relaxed as the transforming interface interacts with second phase particles, defects or other martensite variants, the experimentally observed transformation strains do not achieve the theoretical values. Indeed, TEM reveals the presence of defects in the unaged material and dislocation activity at the interface between two martensite variants in the aged condition.

When the two-way shape memory effect (TWSME) strain was evaluated, differences in the aged versus unaged are again notable. Both samples indicated significant amounts of TWSME strain after thermal cycling (figure 3). Especially in the unaged case, the magnitude of the TWSME strain is nearly 60% of the theoretical strain. It is well known, that internal stresses attributed to residual martensite and oriented dislocation arrays that remain after transformation cycling give rise to the two-way shape memory effect [8]. We observe higher strains in the unaged case because more of the matrix undergoes the transformation. The unaged response displays lower detwinning stresses and less hardening (figure 2), which indicates a lower resistance to twin boundary motion and promotes higher TWSME strains for the unaged condition, respectively. The high volume fraction of fine twins initially present in the aged material reorients, thus reducing the amount of material that undergoes the phase transformation from austenite to martensite. In addition, smaller TWSME strains result for the aged case because of interaction between the high volume fraction of reorienting martensite with the transforming austenite. As a result, the transformation proceeds in a more reversible manner and the hysteresis is smaller. The unaged sample possesses higher hysteresis for the TWSME response, consistent with higher dissipation for the softer matrix case due to dislocation emission at transforming interfaces and stacking faults as shown in the TEM images. Similar to DSC results, the decrease in TWSME thermal hysteresis and TEM indicated defect reductions for the aged specimens suggest that the atomic order is indeed enhanced by aging and that the effect remains after cyclic deformation.

## 5. Conclusions

This work supports the following conclusions:

(1) The critical stress to initiate martensite motion is in the range of 5 MPa at 75 °C for the unaged material. The magnitude of the detwinning stress increases with aging at 850 and 900 °C to levels exceeding 10 MPa.
(2) Aging at 850 and 900 °C produces a finer martensite plate and twin lamellae size consistent with the increased detwinning stress. Apparent microstructural defects are also reduced by aging.
(3) The stress required to induce a phase transformation from austenite to martensite with maximum transformation strains of 5.2% has been established to be 25 and 60 MPa for the unaged and aged cases, respectively.
(4) Remarkably, the thermal hysteresis is as low as 2 °C for the unaged case illustrating the potential utility of these materials as shape memory materials without magnetic fields.

## Acknowledgments

The work was supported by the NSF grant CMS-0428428. Professor Chumlyakov acknowledges RFFI 05-08-17915a, 06-08-08011.

## References

[1] Webster P J, Ziebeck K R A, Towm S L and Pesk M S 1984 *Phil. Mag.* B **49** 295
[2] Vasil'ev A N, Kokorin V V, Savchenko Yu I and Chernenko V A 1990 *Sov. Phys.—JETP* **71** 803
[3] Sozinov A, Likhachev A A, Lanska N, Söderberg O, Koho K, Ullakko K and Lindroos V K 2004 *J. Physique* IV **115** 121
[4] Martynov V V and Kokorin V V 1992 *J. Physique* III **2** 739
[5] Wang W H, Liu Z H, Shan Z W, Chen J L, Wu G H and Zhan W S 2002 *J. Phys. D: Appl. Phys.* **35** 492
[6] Kira T, Murata K, Shimada T, Jeong S, Inoue S, Koterazawa K and Inoue K 2003 *Mater. Sci. Forum* **426–432** 2207
[7] Pons J, Chernenko V A, Cesari E and L'vov V A 2003 *J. Physique* IV **112** 939
[8] Hamilton R F, Sehitoglu H, Chumlyakov Y and Maier H J 2004 *Acta Mater.* **52** 3383
[9] Otsuka K and Wayman C M 1998 *Shape Memory Materials* (Cambridge: Cambridge University Press)
[10] Jin X, Marioni M, Bono D, Allen S M, O'Handley R C and Hsu T Y 2002 *J. Appl. Phys.* **91** 8222
[11] Wang Z G, Zu X T and Huo Y 2005 *Thermochim. Acta* **436** 153
[12] Overholser R W, Wuttig M and Neumann D A 1999 *Scr. Mater.* **40** 1095
[13] Gao Z Y, Zhao X K, Chen F, Cai W, Zhao L C, Wu G H, Chen J L and Zhan W S 2003 *Mater. Sci. Technol.* **19** 691
[14] Ma Y Q, Jiang C B, Feng G and Xu H B 2003 *Scr. Mater.* **48** 365
[15] Pirge G, Hyatt C V and Altıntaş S 2004 *J. Mater. Proc. Technol.* **155/156** 1266
[16] Wu S K and Yang S T 2003 *Mater. Lett.* **57** 4291
[17] Segui C, Chernenko V A, Pons J and Cesari E 2003 *J. Physique* IV **112** 903
[18] Khovailo V V, Kainuma R, Abe T, Oikawa K and Takagi T 2004 *Scr. Mater.* **51** 13
[19] Hosoda H, Wakashima K, Sugimoto T and Miyazaki S 2002 *Mater. Trans. JIM* **43** 852
[20] Bhattacharya K 2003 *Microstructure of Martensite: Why It Forms and How It Gives Rise to the Shape-Memory Effect* (New York: Oxford University Press)
[21] Sehitoglu H, Zhang X Y, Kotil T, Canadinc D, Chumlyakov Y and Maier H J 2002 *Metall. Mater. Trans.* A **33A** 3661
[22] Ball J M and James R D 1987 *Arch. Ration. Mech. Anal.* **100** 13
[23] Sehitoglu H, Karaman I, Zhang X Y, Chumlyakov Y and Maier H J 2001 *Scr. Mater.* **44** 779
[24] Karaca H E, Karaman I, Chumlyakov Y I, Lagoudas D C and Zhang X 2004 *Scr. Mater.* **51** 261
[25] Hamilton R F, Sehitoglu H, Efstathiou C, Maier H J, Chumlyakov Y and Zhang X Y 2005 *Scr. Mater.* **53** 131
[26] Bennett J C, Hyatt C V, Gharghouri Ma, Farrell S, Robertson M, Chen J and Pirge G 2004 *Mater. Sci. Eng.* A **378** 409
[27] Ling H C and Owen W S 1981 *Acta Metall.* **29** 1721
[28] Khan A Q, Brabers M and Delaey L 1974 *Mater. Sci. Eng.* **15** 263
[29] Söderberg O, Ge Y, Sozinov A, Hannula S P and Lindroos V K 2005 *Smart Mater. Struct.* **14** S223
[30] Pons J, Chernenko V A, Santamarta R and Cesari E 2000 *Acta Mater.* **48** 3027